An Efficient Aggregation-Enhanced Delayed Fluorescence Luminogen Created with Spiro Donors and Carbonyl Acceptor for the Applications as Emitter and Sensitizer in High-Performance OLEDs

Hao Chen, Jiajie Zeng, Ruishan Huang, Jianghui Wang, Junchu He, Hao Liu, Dezhi Yang, Dongge Ma, Zujin Zhao and Ben Zhong Tang*

H. Chen, J. Zeng, R. Huang, J. Wang, J. He, H Liu, D. Yang, Dr. D. Ma, Prof. Z. Zhao, Prof. B. Z. Tang
State Key Laboratory of Luminescent Materials and Devices, Guangdong Provincial Key Laboratory of Luminescence from Molecular Aggregates, South China University of Technology, Guangzhou 510640, China.
E-mail: mszjzhao@scut.edu.cn
Prof. B. Z. Tang
School of Science and Engineering, Shenzhen Institute of Aggregate Science and Technology, The Chinese University of Hong Kong, Shenzhen, Guangdong 518172, China
Prof. B. Z. Tang
AIE Institute, Guangzhou Development District, Huangpu, Guangzhou 510530, China.

Keywords: aggregation-enhanced emission, thermally activated delayed fluorescence, bipolar carrier transport, sensitizer, organic light-emitting diode

Abstract: Organic light-emitting diodes (OLEDs) fabricated using organic thermally activated delayed fluorescence materials as sensitizers have achieved significant advancements recently, but the serious efficiency roll-offs are still troublesome in most cases. Herein, a tailor-made multifunctional luminogen SBF-BP-SFAC containing 9,9'-spirobifluorene and spiro[acridine-9,9-fluorene] as electron-donors and carbonyl as electron-acceptor is synthesized and characterized. SBF-BP-SFAC holds advantages of high thermal stability, aggregation-enhanced delayed fluorescence, balanced carrier transport ability and prefers horizontal dipole orientation. Highly efficient OLEDs employing SBF-BP-SFAC as emitter radiate intense cyan light and outstanding external quantum efficiencies (η_{ext}s) of up to 30.6%. SBF-BP-SFAC can also serve as an excellent sensitizer for orange fluorescence, phosphorescence and delayed fluorescence materials, providing excellent η_{ext}s of up to 30.3% with very small efficiency roll-offs due to the fast Förster energy transfer as well as the exciton annihilation suppression by bulky spiro donors. These outstanding performances demonstrate the great potential of SBF-BP-SFAC as emitter and sensitizer for OLEDs.

1. Introduction

Organic light-emitting diodes (OLEDs) as a hotpoint in displays and white illumination devices have been applied gradually in recent years because of flexibility, high color quality and low

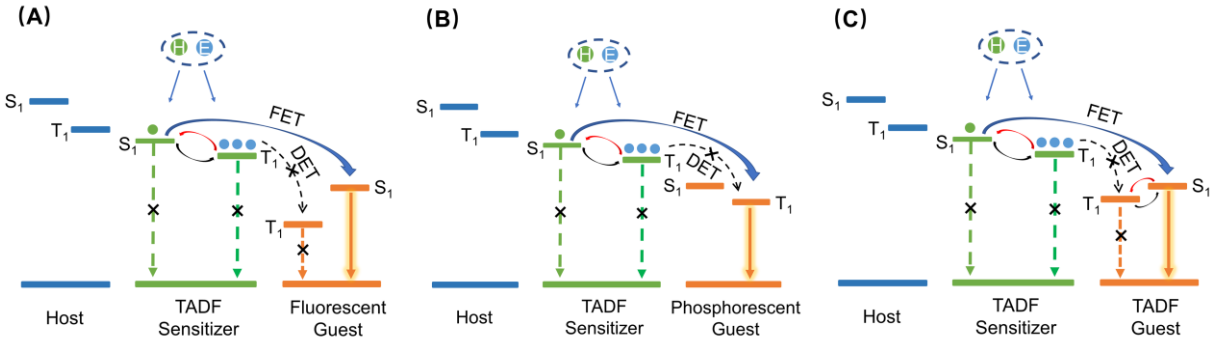

Figure 1. Schematic of the energy transfer mechanisms in sensitized OLEDs for fluorescent guest (A), phospherescent guest (B) and TADF guest (C).

energy cost, and the development of robust organic luminescent materials for OLEDs becomes particularly important.[1] Thermally activated delayed fluorescence (TADF) luminogens generally consist of organic donor (D) and acceptor (A) with a highly twisted connection, which can utilize 100% singlet and triplet electro-generated excitons via a reverse intersystem crossing (RISC) process to achieve outstanding electroluminescence (EL) efficiencies in OLEDs. The small energy gap (ΔE_{ST}) from the lowest excited triplet state (T_1) to the lowest excited singlet state (S_1) is the key for the occurrence of RISC process, which can be facilely achieved by molecular designs to sufficiently restrict the overlap between the highest occupied molecular orbital (HOMO) and the lowest unoccupied molecular orbital (LUMO).[2] So far, TADF emitters are emerging as the 3rd generation luminescent materials for OLEDs,[3] and have furnished excellent EL performances for full-color OLEDs and white OLEDs.[4] Besides, some TADF materials can also be used as sensitizers for fluorescence, phosphorescence and TADF emitters, providing new strategies for the fabrication of OLEDs with high efficiencies,[5] but the large efficiency roll-offs remain a thorny problem in most cases. As shown in Figure 1, the TADF sensitizers in these sensitized devices act as the main carrier recombination centers. The T_1 excitons of TADF sensitizers are upconverted to S_1 excitons and then transferred to the S_1 excitons of the guest emitters via long-distance Förster energy transfer (FET) to realize theoretical 100% exciton utilization efficiency.[6] In order to ensure high FET efficiencies in the sensitized devices, choosing appropriate sensitizer and guest emitter to maximize the spectral overlap between the photoluminescence (PL) spectrum of the sensitizer and the absorption spectrum of the guest emitter is of high importance.[7] Meanwhile, in this blended system of sensitizer and guest emitter, it is necessary to keep sufficient intermolecular distances to suppress exchange and quenching of the triplet excitons via Dexter energy transfer (DET), which is usually realized by employing bulky substituents or lowering doping concertation.[8] By this way, it is envisioned that efficient sensitized device can be achieved through fast and

efficient energy transfer process, balanced carrier transportation, as well as inhibited triplet–polaron quenching (TPQ) and triplet–triplet annihilation (TTA) in the emitting layers.[9]

As discussed above, TADF sensitizers play a promising role in creating high EL efficiency sensitized OLEDs while a majority of TADF sensitizers experience serious emission quenching and exciton annihilation, which greatly undermine device performance and practial application. To meet the above needs and challenges, Aggregation-Enhanced Delayed Fluorescence (AEDF) luminogen was demonstrated to be an efficient candidate. Previously, we developed a luminogen SBF-BP-DMAC with evident aggregation-enhanced emission (AEE) and TADF character, which achieved high external quantum efficiency (η_{ext}) of 24.5% as emitter and 26.8% as sensitizer for Ir(tptpy)$_2$acac.[10] This achievement greatly promoted the development of multifunctional delayed fluorescence materials acting as both emitter and sensitizer. In this work, we further optimize the above work in molecular engineering and device structure. Firstly, we replace a donor group in the molecule from DMAC to SFAC, which was demonstrated to be conducive to facilitating horizontal orientation of the emitting dipole.[11] Based on the optical outcoupling efficiency (η_{out}) of 34.9%, the maximum η_{ext} of doped devices with SBF-BP-SFAC as emitter is increased to 30.6%. Meanwhile, because of the electron donating ability of the SFAC group is weaker than that of the DMAC group, the spectrum of the molecule is blue shifted from green to cyan. SBF-BP-SFAC with similar D-A-D' structure maintains evident AEE and TADF characteristics as well as the advantages of small ΔE_{ST} value and bipolar carrier transport capicity. Besides, the introduction of SBF and SFAC as bulky functional units can not only enhance molecular rigidity and stability but also increase the intermolecular distance between the sensitizer and the emitter to alleviate emission quenching and exciton annihilation in solid state. Secondly, we further improve the performance of SBF-BP-SFAC as the sensitizer for guest emitter by optimizing the device structure that the maximum η_{ext} of doped device for Ir(tptpy)$_2$acac is increased from 26.8% to 30.3%. We have also expanded the types of guest emitterss for SBF-BP-SFAC sensitizer, including fluorescence, phosphorescence as well as TADF emitters. They all achieved outstanding η_{ext}s and small efficiency roll-offs, validating that SBF-BP-SFAC can serve as a potential emitter and sensitizer for OLEDs. Finally, we systematically study the energy transfer process of the sensitized devices by exciton dynamics analysis that the the larger FET radium (R_0), the faster FET rate (k_{FET}) and higher FET efficiency (Φ_{FET}) can prove the rationality of the device performance improvement strongly.

2. Results and Discussion

2.1 Synthesis and Characterization

The synthetic procedure and structure of the target molecule are presented in Scheme 1. The molecule SBF-BP-SFAC as cyan emitter was synthesized by two-step reactions with 87% yield. The chemical structure was comprehensively confirmed and the characterization data are listed in Supporting Information. The thermogravimetric analysis (TGA) and differential scanning calorimetry (DSC) measurement (Figure 2A) reveal it possesses high decomposition temperature (T_d, at 5% weight loss) of 442 °C and glass-transition temperature (T_g) of 163 °C, suggesting its excellent thermal and morphological stability for the OLEDs fabrication via vacuum doposition.

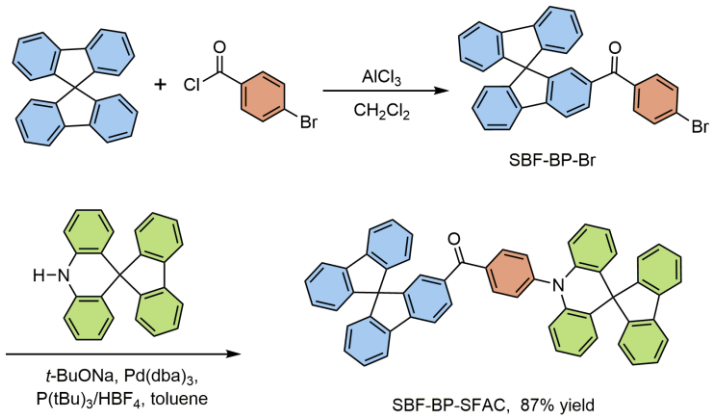

Scheme 1. Synthetic route and chemical structure of SBF-BP-SFAC.

To confirm the structure and investigate the intermolecular interaction of SBF-BP-SFAC, the single crystals were cultured by solvent vapor diffusion in the dichloromethane/*n*-hexaneat mixture, and crystal structure was determined by X-ray single crystallography method. It can be found in Figure 3A that SBF-BP-SFAC adopts a highly torsional geometry with a big dihedral angle of 82.22° between SFAC moiety and the adjacent phenyl group. Such a twisted conformation can effectively suppress the spatial overlap between the HOMO and LUMO to generate a small ΔE_{ST}, and meanwhile contributate to inhibiting close molecular packing to alleviate energy dissipation in the aggregated state. Besides, according to the packing pattern

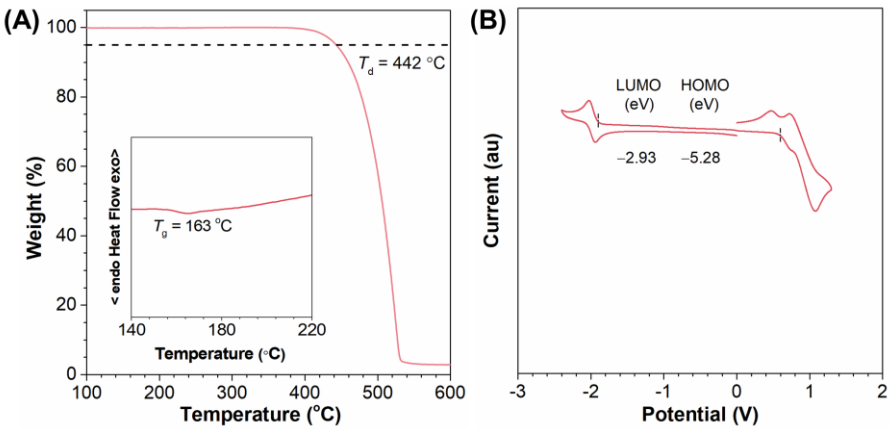

Figure 2. (A) TGA and DSC curves and (B) CV curve of SBF-BP-SFAC.

of SBF-BP-SFAC in crystals (Figure 3B), there are no obviously close π–π stacking interactions but abundant C−H···π interactions (2.690−3.183 Å) and C−H···O interactions (2.419 Å), which is beneficial for enhancing the molecular rigidify and restricting intramolecular motion to reduce the energy loss through nonradiative decay channels, thus promonting emission efficiency in solid states.

2.2 Electronic Structures and Energy Levels

Theoretical calculation was performed to investigate the geometrical structure, frontier molecular orbitals and predict ΔE_{ST} of SBF-BP-SFAC. The optimized molecular structure of SBF-BP-SFAC is highly twisted, similar to the crystal strucutre. The HOMO is primarily distributed on the acridine segment while the LUMO is mainly dispersed over carbonyl core and adjacent phenyl and carbazole units (Figure 3C). The completely separated distribution of HOMO and LUMO indicates a small theoretical ΔE_{ST} of SBF-BP-SFAC. Accordig to the optimized ground-state geometry, the ΔE_{ST} value is calculated as small as 0.11 eV, ensuring the occurrence of RISC process to generate the delayed fluorescence. To obtain the electrochemical property of SBF-BP-SFAC, cyclic voltammetry (CV) was conducted in the solutions (Figure 2B). The initial potentials of oxidation and reduction against Fc/Fc^+ redox couple are 0.48 and −1.87 V, respectively. Therefore, the energy levels of HOMO and LUMO were calculated to be about −5.28 and −2.93 eV, respectively, according to the onsets of

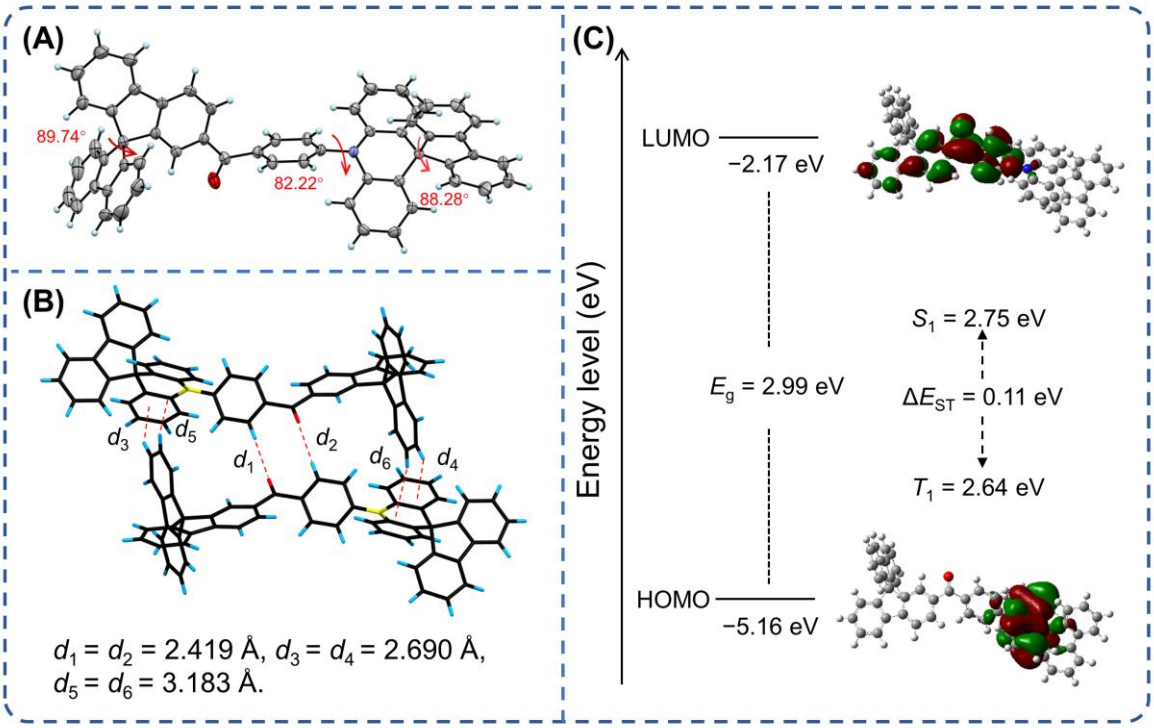

Figure 3. (A) Single crystal structure and (B) packing diagram of SBF-BP-SFAC (CCDC: 1947781). (C) Frontier molecular orbital distribution and energy level of SBF-BP-SFAC.

oxidation and reduction waves (HOMO = −[E_{ox} + 4.8] eV; LUMO = −[E_{re} + 4.8] eV, where E_{ox} and E_{re} represent the onset potentials of oxidation and reduction potentials of SBF-BP-SFAC relative to Fc/Fc^+, respectively). The appropriate energy levels are applicable for the injection of hole and electron in OLEDs.

2.3 Photophysical Properties

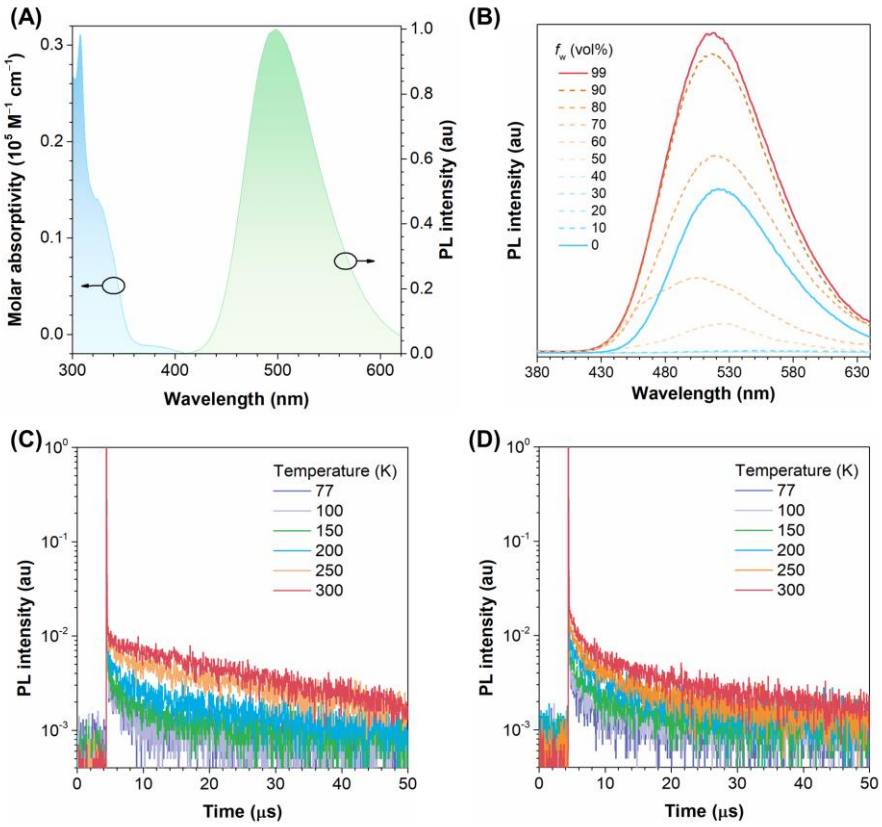

Figure 4. (A) UV-vis absorption spectrum in THF solution (10^{-5} M) and photoluminescence (PL) spectrum in neat film. (B) PL spectra in THF/water binary solutions with varied f_w (10^{-5} M) from 0% to 99%. Transient PL decay curves of SBF-BP-SFAC in (C) nondoped and (D) doped film at the temperatures from 77 K to 300 K.

The photophysical properties of SBF-BP-SFAC was investigated in THF solution with a concentration of 10^{-5} M. As shown in Figure 4A, SBF-BP-SFAC possesses an absorption peak around 328 nm assigned to the π–π* transition of the D–A unit. Meanwhile, a weak wide absorption tail at long wavelengths is observed till 410 nm, which can be attributed to the intramolecular charge transfer (ICT) state from SFAC group to carbonyl core. In THF solution, SBF-BP-SFAC shows weak green PL emission at 521 nm with a relatively low PL quantum efficiency (Φ_{PL}) of 22.5%. When a small volume of water (as poor solvent) is added to the THF solution, the PL intensity is weakened to some extent. It can be ascribed to the enhanced ICT effect with the increased polarity of the mixed solvents. But the PL intensity increases significantly as the water fraction (f_w) of the mixture is beyond 80 vol% (Figure 4B). This

phenomenon of AEE can be attributed to the aggregate formation in almost aqueous environment, which can restrict the intramolecular vibrations and rotations to suppress the nonradiative decay in the excited state.[12] In comparison with THF solution, the vacuum deposition film of SBF-BP-SFAC shows a bluer emission at 498 nm, with a high Φ_{PL} of 71.1%. Similarly, the doped film of SBF-BP-SFAC in (bis-(diphenylphosphoryl)-dibenzo[b,d]-furan (PPF) host with a doping concentration of 30 wt% also shows a blue-shifted emission peak at 506 nm with a higher Φ_{PL} of 94.6%. The bluer and stronger PL emissions in both neat and doped films can be partially ascribed to the reduction of the polarity in the films and restriction of intramolecular motion, which further validate the AEE characteristic of SBF-BP-SFAC as well.

Table 1. Summary of the photophysical data of SBF-BP-SFAC.

	solution[a)]	neat film[b)]	doped film[b)]
λ_{abs} [nm]	328	324	320
λ_{em} [nm]	521	498	506
Φ_{PL}[c)] [%]	22.5	71.1	94.6
$<\tau>$[d)] [ns]	279.5	12246.3	7792
τ_{prompt}[e)] [ns]	19.8	24.2	27.6
$\tau_{delayed}$[e)] [μs]	2.5	23.8	17.4
$R_{delayed}$[f)] [%]	10.6	51.4	44.7
ΔE_{ST}[g)] [eV]	-	0.028	0.024

[a)]Collected in THF solution (10^{-5} M); [b)]Measured in neat film and doped film (30 wt% SBF-BP-SFAC: PPF); [c)]Absolute PL quantum yield; [d)]Mean fluorescence lifetime evaluated at room temperature; [e)]PL lifetime of the prompt fluorescence and delayed component; [f)]Ratio of delayed component; [g)]Energy gap between S_1 and T_1.

SBF-BP-SFAC shows similar prompt fluorescence lifetimes in the range of 19.8–27.6 ns in THF solution, and neat and doped films. But the latter two states exhibit much longer delayed fluorescence lifetimes of 23.8 and 17.4 μs, respectively, with much higher ratios of delayed components, than THF solution (2.5 μs) (Table 1), indicating SBF-BP-SFAC has promoted delayed fluorescence in vacuum deposition film. To further confirm the delayed fluorescence property of SBF-BP-SFAC, the transient PL behaviors under diffent temperature were examined for the neat and doped films in nitrogen atmosphere. As depicted in Figure 4C and 4D, the decay of PL intensity increases apparently as the temperature rises from 77 K to 300 K, as the result of the promoted RISC process under thermal activation, validating typical TADF characteristic.[13] Combining the evident AEE and TADF properties, SBF-BP-SFAC possesses interesting aggregation-enhanced delayed fluorescence nature. The low-temperature (77 K)

fluorescence and phosphorescence spectra were collected (Figure S1, Supporting Information), and the triplet energy levels of SBF-BP-SFAC were calculated to be 2.618 and 2.637 eV in neat and doped films, respectively. Therefore, the ΔE_{ST} values are as small as 0.028 and 0.024 eV for SBF-BP-SFAC in neat and doped films, which are conducive to accelerating RISC process and acquiring efficient delayed fluorescence in aggregared states.

2.4 Electroluminescence Performance

2.4.1 OLEDs with SBF-BP-SFAC as Emitter

To investigate the EL property of SBF-BP-SFAC, nondoped and doped OLED devices were fabricated via vacuum deposition technique with the multilayer configuration of Figure 5A, in which neat film of SBF-BP-SFAC functions as emitting layer (EML) for nondoped device (device I) and doped film of 30 wt% SBF-BP-SFAC in PPF host functions as EML for doped device (device II). The low turn-on voltages (V) at 3.0 V is obtained for both devices and the devices illuminate strong cyan light around 506−510 nm with maximum luminance (L) beyond 30000 cd m^{-2} (Table 2). For nondoped device I, the maximum current efficiency (η_C), power efficiency (η_P), and η_{ext} are achieved as 65.0 cd A^{-1}, 61.7 lm W^{-1} and 23.1%, respectively. For doped device II, the maximum η_C, η_P, and η_{ext} are increased to 83.3 cd A^{-1}, 74.3 lm W^{-1} and 30.6%, respectively, due to the higher Φ_{PL} of SBF-BP-SFAC in doped film. To understand the

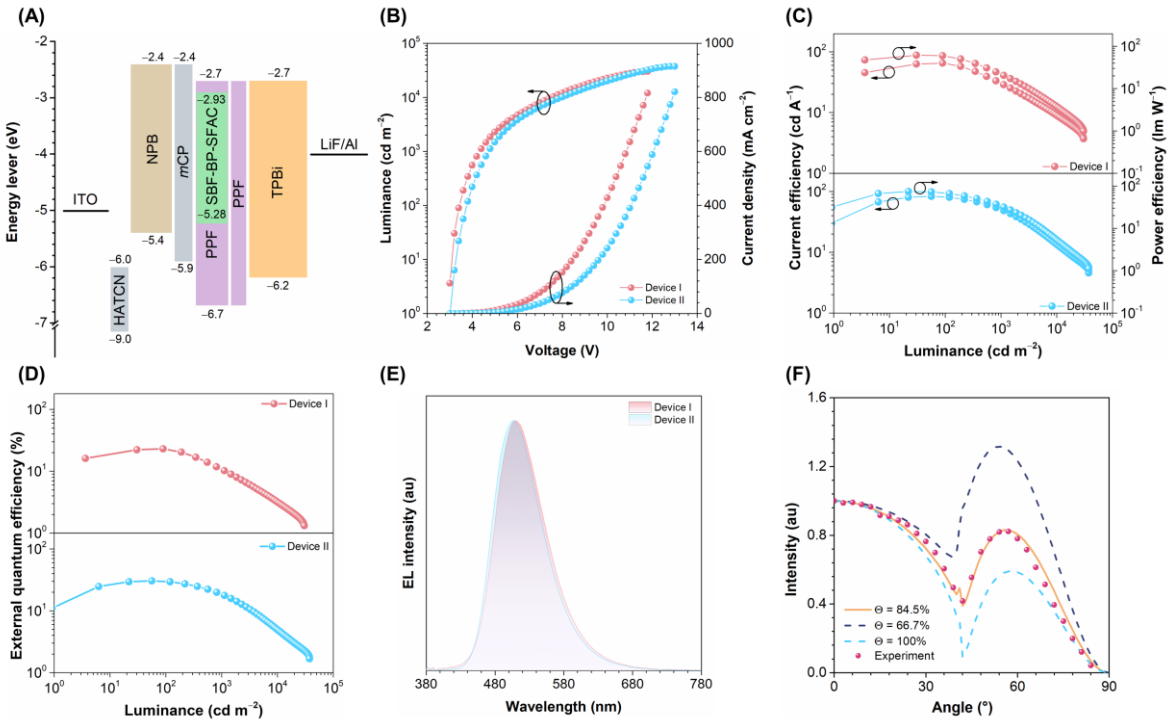

Figure 5. (A) Schematic energy-level diagram of nondoped (I) and doped (II) devices. Plots of (B) L–V–current density (J), (C) η_C–L–η_P, (D) η_{ext}–L, and (E) EL spectra at 10 mA cm^{-2} of the devices. (F) Variable-angle PL measurements of 30 wt% SBF-BP-SFAC doped in PPF film.

outstanding EL performance, the ratio of horizontal orientation emitting dipole (Θ//) of SBF-BP-SFAC in doped film is investigated by variable-angle *p*-polarized PL measurement (Supporting Information) and the result is shown in Figure 5F. The $\Theta_{//}$ of SBF-BP-SFAC doped film are fitted to be 84.5%, indicating it prefers horizontal dipole orientation. According to the Θ//, reflex indexes and thickness of active layers, the η_{out} of an optimized doped OLED with SBF-BP-SFAC as emitter was calculated to be 34.9%. Therefore, the high Φ_{PL}, η_{out} and exciton utilization account for the superb EL performance of SBF-BP-SFAC in doped device.

Table 2. Summary of performance data of OLEDs with SBF-BP-SFAC as emetters.

Device	V_{on} [V][a)]	L_{max} [cd m^{-2}][b)]	$\eta_{C,max}$ [cd A^{-1}][c)]	$\eta_{P,max}$ [lm W^{-1}][d)]	$\eta_{ext,max}$ [%][e)]	λ_{EL} [nm][f)]	CIE (x, y)[g)]
I[h)]	3.0	30299	65.0	61.7	23.1	510	(0.230, 0.499)
II[h)]	3.0	37520	83.3	74.3	30.6	506	(0.217, 0.480)

[a)]Operating voltage at 1 cd m^{-2}; Maximum [b)]luminance, [c)]current efficiency, [d)]power efficiency and [e)]external quantum efficiency; [f)]EL emission wavelength peak at 10 mA cm^{-2}; [g)]Commission Internationale de I'Eclairage 1931 coordinates at 10 mA cm^{-2}; [h)]Emitting layers for device I and II are the SBF-BP-SFAC and 30 wt% SBF-BP-SFAC: PPF, respectively.

2.4.2 Carrier Transport Capacity

Balanced carrier transport is of great importance to gain high EL performances of the devices. In view of the excellent EL efficiencies in nondoped and doped devices with SBF-BP-SFAC as emitter, the electron-only device (EOD) and the hole-only devices (HOD) were fabricated to measure its carrier mobility property via space-charge-limited current (SCLC) method (Supporting Information).[14, 15] The thin layers of TmPyPB with an electron mobility (μ_e) of about 10^{-3} cm^2 V^{-1}s^{-1}[16] and TAPC with a hole mobility (μ_h) of about 10^{-2} cm^2 V^{-1}s^{-1}[17] were used as electron/hole-injection layer and hole/electron-blocking layer between emissive layer and the electrodes. The current density versus the applied voltage of the EOD and HOD are shown in Figure 6A and the electric field-dependent mobilities (μ) is illustrated in Figure 6C.

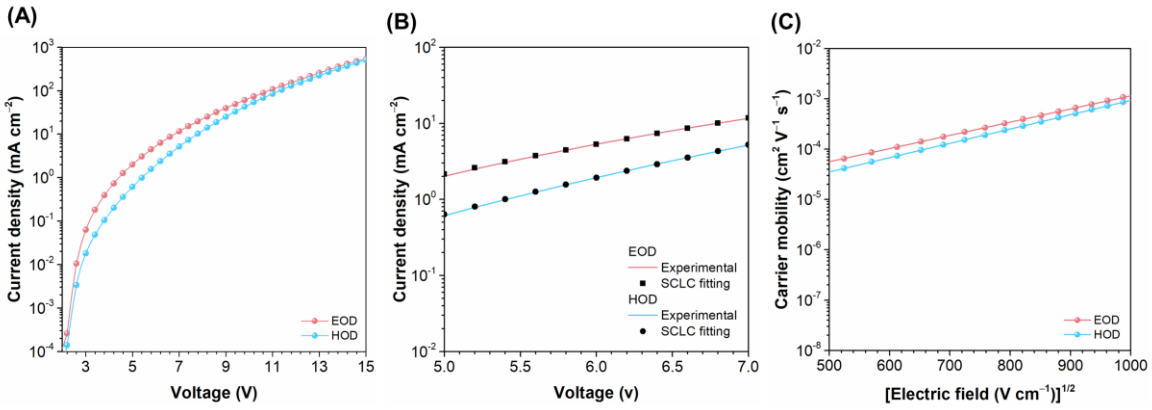

Figure 6. (A) *J*–*V* curves of the EOD and HOD for SBF-BP-SFAC. (B) SCLC fitting of EOD and HOD. (C) Carrier mobility–electric field curves of SBF-BP-SFAC.

The results reveal that SBF-BP-SFAC features noticeable bipolar carrier transport ability at opeational voltage region with very close μ_e of and μ_h of 1.96×10^{-4} and 1.72×10^{-4} cm^2 V^{-1} s^{-1}, respectively, at a practical electric field of 5.5×10^5 V cm^{-1}. It is beneficial to balance the carrier transportation, enhance the EL perfmance and suppress the efficiency roll-off in OLED devices.

2.4.3 OLEDs with SBF-BP-SFAC as Sensitizer

With the excellent aggregation-enhanced delayed fluorescence property and balanced carrier transport capacity, the potential of SBF-BP-SFAC as sensitizer for orange fluorescence, phosphorescence and TADF emitters of TBRb, phosphorescent It(tptpy)$_2$acac and 4CzTPN-Ph, respectively, are evaluated (Figure 7A). The UV–vis absorption spectra of guest emitters overlap well with the PL wavelength of SBF-BP-SFAC (Figure 7B), which is favorable to achieve efficient FET from SBF-BP-SFAC to these emitters. Multilayer sensitized OLEDs

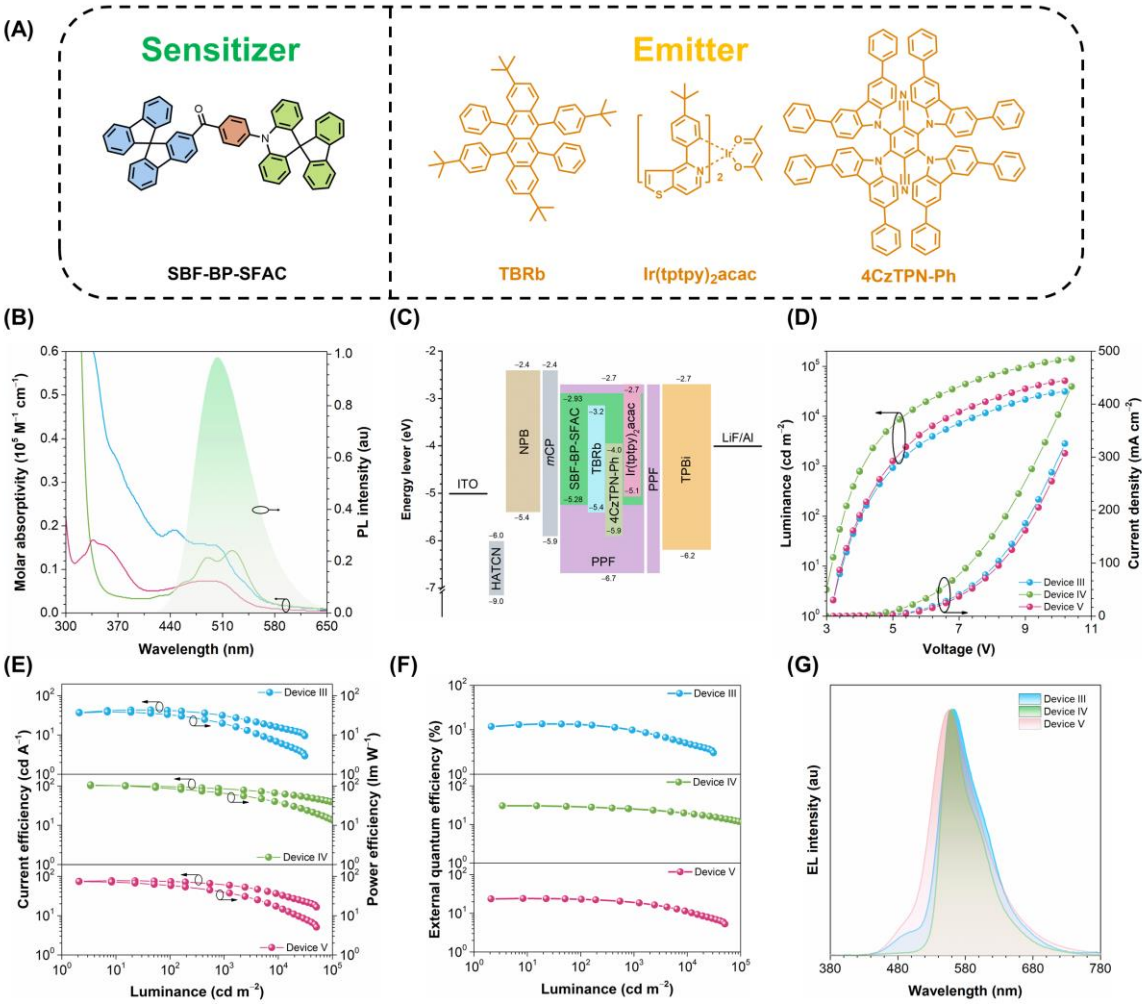

Figure 7. (A) Chemical structures of the sensitizer SBF-BP-SFAC and orange guest emitters. (B) Absorption spectra of orange guest emitters in films and PL spectrum of SBF-BP-SFAC in doped film. (C) Schematic energy-level diagram of the sensitized OLEDs with SBF-BP-SFAC as sensitizer. Plots of (D) *L*–*V*–*J*, (E) η_C–*L*–η_P, (F) η_{ext}–*L*, and (G) EL spectra at 10 mA cm^{-2} of the devices.

were fabricated with the configurations in Figure 7C, where the EML is composed by the doped films of PPF host containing 30 wt% SBF-BP-SFAC and 1 wt% TBRb for device III, 30 wt% SBF-BP-SFAC and 3 wt% It(tptpy)$_2$acac for device IV, and 30 wt% SBF-BP-SFAC and 1 wt% 4CzTPN-Ph for device V. The energy level diagrams of the sensitized OLED devices are depicted in Figure 7C and the summarized EL performances are shown in Table 3. These devices can be turned on at low voltages of 2.9–3.2 V and provide orange lights with peaks at around 560 nm, indicating efficient charge injection and transportation as well as sufficient FET from the sensitizer to the emitters are successfully achieved in these devices. These devices afford peak luminance of 31060, 140700, 50990 cd m^{-2} and maximum η_{ext}s of 13.6%, 30.3%, 24.2%, respectively. The η_{ext} of device III with TBRb as emitter is enhanced by more than two folds relative to those of traditional devices and the η_{ext} of device V with 4CzTPN-Ph as emitter is the highest η_{ext} ever reported for 4CzTPN-Ph (Table S1, Supporting Information). Besides, these devices still maintain good EL performance with η_{ext} of 10.0%, 25.6% and 18.6% at 1000 cd m^{-2}, respectively, indicative of small efficiency roll-offs. All above outstanding EL performances demonstrate that SBF-BP-SFAC can function as an excellent sensitizer for orange emitters.

Table 3. Summary of performance data of OLEDs with SBF-BP-SFAC as sensitizer.

Device[a)]	V_{on} [V]	L_{max} [cd m^{-2}]	Maximum $\eta_{ext}/\eta_C/\eta_P$ [%/cd A^{-1}/lm W^{-1}]	$\eta_{ext}/\eta_C/\eta_P$ at 1000 cd m^{-2} [%/cd A^{-1}/lm W^{-1}]	λ_{EL} [nm]	CIE (x, y)
III[f)]	3.2	31060	13.6/43.3/38.4	10.0/31.5/20.0	562	(0.441, 0.511)
IV[f)]	2.9	140700	30.3/102.1/106.7	25.6/86.2/67.7	560	(0.470, 0.520)
V[f)]	3.2	50990	24.2/77.4/73.4	18.6/59.5/37.4	556	(0.423, 0.535)

[a)]The emitting layers for device III, IV and V are 1 wt% TBRb: 30 wt% SBF-BP-SFAC: PPF, 3 wt% It(tptpy)$_2$acac: 30 wt% SBF-BP-SFAC: PPF and 1 wt% 4CzTPN-Ph: 30 wt% SBF-BP-SFAC: PPF, respectively.

2.4.4 Mechanistic Studies of Sensitized OLEDs

In view of the satisfactory EL peformance and small efficiency roll-offs of these sensitized OLEDs, it's meaningful to further explore the process of energy transfer and the mechanism of efficiency attenuation. It can be found from the schematic energy levels in Figure 7C that the HOMO level of SBF-BP-SFAC is much shallower than that of PPF host, indicating that SBF-BP-SFAC can trap holes to comfine charge recombination within the sensitizer instead of the emitters. The sensitizer SBF-BP-SFAC can harvest 100% excitons by converting triplet excitons to singlet excitons, and then excite the guests through efficient long-distance FET process to acquire high EL efficiencies of the guests. To investigate the exciton behavior of these sensitized OLEDs, the exciton recombination zones of devices III−V were studied. The R_0 theoretical k_{FET} and Φ_{FET} were determined according to previously reported method

(Supporting Information).[18] All the calculated data are presented in Table 4. It can be found that the k_{FET}s in the EMLs of three sensitized OLEDs are calculated as 1.81−5.95 × 10^8 s^{-1} and the Φ_{FET}s are 83.3%−93.4%, demonstrating the fast rate and high efficiency of FET. Besides, the distance between the sensitizer and the doped emitters are 2.22−3.11 nm, indicating the low concentration doping technique has weakened the DET (effective transmission distance are 1−1.5 nm).[19] Therefore, the long-distance FET from the sensitizer SBF-BP-SFAC to the emitters predominantly contributes to the outstanding EL efficiencies of the sensitized OLEDs.

Table 4. Summary of energy transfer parameters of the sensitized OLEDs.

Device[a)]	R_0 [nm][b)]	R_{hg} [nm][c)]	R_{gg} [nm][d)]	k_{FET} [× 10^8 s^{-1}][e)]	Φ_{FET} [%][f)]
III	4.06	3.11	5.00	1.81	83.3
IV	3.44	2.22	3.60	5.95	93.4
V	3.69	2.64	4.30	2.69	88.1

[a)]FET radius; [b)]Distance between the host (h) and guest (g); [c)]Distance between two guests; [e)]FET rate; [f)]FET efficiency.

These above sensitized OLEDs exhibit not only high efficiencies but also small efficiency roll-offs at high current density. Actually, there are many factors leading to efficiency degradation of the OLEDs, such as TTA and TPQ. To deeply understand the efficiency decay mechanism of these sensitized devices, the curves of η_{ext} and J of these devices III−V are fitted by the TTA model[20] and TPQ model.[21] The TTA simulation can be described as equations 1, where η, η_0, and J_0 represent the η_{ext} in the presence of TTA, initial η_{ext} in the absence of TTA (TTA quenching is ideally negligible at very low current density), and the current density at the half-maximum of η_{ext}, respectively. The TPQ simulation can be described as equation 2, where η_0 is the η_{ext} in the absence of TPQ, C is a constant which is related to the parameters like dielectric constant, carrier mobility, TPQ rate constant and decay lifetime. To obtain a good fitting result, it requires that l equals to 1 which means that the charge transport in device should follow SCLC characteristic.

$$\frac{\eta}{\eta_0} = \frac{J_0}{4J}\left(\sqrt{1+8\frac{J}{J_0}}-1\right) \quad (1)$$

$$\frac{\eta}{\eta_0} = \frac{1}{1+CJ^{\frac{1}{l}+1}} \quad (2)$$

As depicted in Figure 8, the results of TTA fitting are coincided well with the practical curves for these sensitized devices, even in the region of high current density, indicating that the TTA process is the prime factor for the efficiency decline of the sensitized devices at high current density. In this sense, the small efficiency roll-off under high current density can be attributed to the alleviation of triplet excitons aggregation via fast FET process and long intermolecular distances due to space-demanded bulky spior donors. On the other hand, the failure of TPQ model fitting implies the well-balanced charge injection and transportation in these sensitized

devices, especially at high current density, which can be partially attributed the well-balanced hole- and electron transport ability of SBF-BP-SFAC.

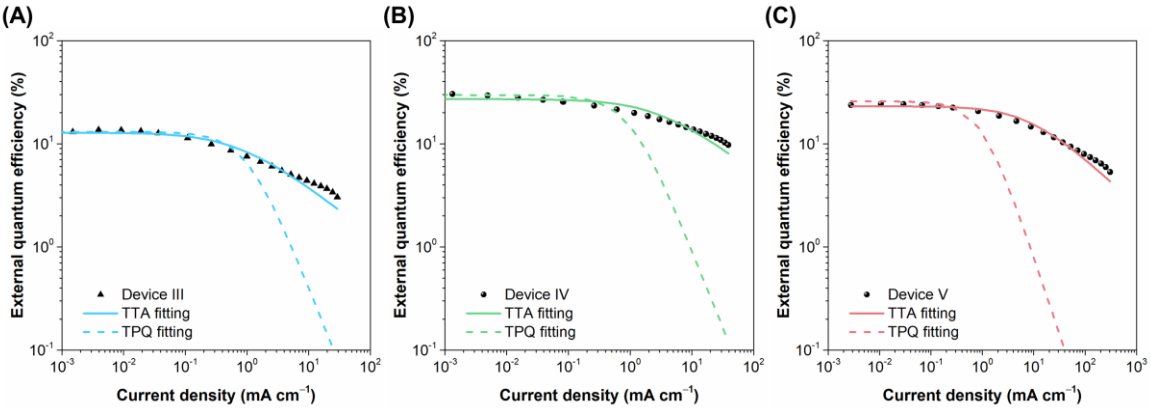

Figure 8. Curves of η_{ext} and J and the corresponding TTA and TPQ fitting curves of devices III−V.

3. Conclusion

In summary, a new multifunctional luminogen SBF-BP-SFAC with the highly twisted configuration of an electron-accepting carbonyl core and two electron-donating spiro groups is successfully synthesized and characterized. SBF-BP-SFAC exhibits high thermal stability, bipolar carrier transport and aggregation-enhanced delayed fluorescence with an excellent Φ_{PL} of 94.6%. Owing to the presence of the spiro acridine donor, SBF-BP-SFAC prefers horizontal orientation with a high $\Theta_{//}$ value of 84.5%, leading to a large η_{out} of 34.9%. The nondoped and doped OLEDs employing SBF-BP-SFAC as emitters provide outstanding maximum η_{ext} values of up to 23.1% and 30.6%, respectively. Besides, SBF-BP-SFAC can also act as an efficient sensitizer for orange fluorescence, phosphorescence and TADF materials, providing excellent EL performance with η_{ext}s of up to 30.3%. The bulky spiro donors can effectively suppress close molecular packing and alleviate the exciton annihilation, and the fast FET rates (10^8 s^{-1}) and high FET efficiencies (93.4%) from SBF-BP-SFAC sensitizer to the guest emitters also efficiently decrease the density of triplet excitons. Both factors work synergistically to result in reduced efficiency roll-offs of the OLEDs. The superior comprehensive EL performance indicates that SBF-BP-SFAC has great application potential in OLEDs as emitter and sensitizer.

Supporting Information

Supporting Information is available from the Wiley Online Library or from the author.

Acknowledgements

This work was financially supported by the National Natural Science Foundation of China (21788102) and the Natural Science Foundation of Guangdong Province (2019B030301003).

Received: ((will be filled in by the editorial staff))
Revised: ((will be filled in by the editorial staff))
Published online: ((will be filled in by the editorial staff))

References

[1] a) C. W. Tang, S. A. VanSlyke, *Appl. Phys. Lett*. **1987**, *51*, 913; b) D. H. Ahn, S. W. Kim, H. Lee, I. J. Ko, D. Karthik, J. Y. Lee, J. H. Kwon, *Nat. Photonics* **2019**, *13*, 540; c)K. Tuong Ly, R.-W. Chen-Cheng, H.-W. Lin, Y.-J. Shiau, S.-H. Liu, P.-T. Chou, C.-S. Tsao, Y.-C. Huang, Y. Chi, *Nat. Photonics* **2016**, *11*, 63; d) C.-Y. Chan, M. Tanaka, Y.-T. Lee, Y.-W. Wong, H. Nakanotani, T. Hatakeyama, C. Adachi, *Nat. Photonics* **2021**, *15*, 203; e) Y. Liu, X. Man, Q. Bai, H. Liu, P. Liu, Y. Fu, D. Hu, P. Lu, Y. Ma, *CCS Chem.* **2022**, *4*, 214.

[2] a) A. Endo, M. Ogasawara, A. Takahashi, D. Yokoyama, Y. Kato, C. Adachi, *Adv. Mater*. **2009**, *21*, 4802; b) D. Zhang, J. Qiao, D. Zhang, L. Duan, *Adv. Mater*. **2017**, *29*, 1702847; c) X. Tang, L. S. Cui, H. C. Li, A. J. Gillett, F. Auras, Y. K. Qu, C. Zhong, S. T. E. Jones, Z. Q. Jiang, R. H. Friend, L. S. Liao, *Nat. Mater.* **2020**, *19*, 1332; d) T. Yang, Z. Cheng, Z. Li, J. Liang, Y. Xu, C. Li, Y. Wang, *Adv. Funct. Mater*. **2020**, *30*, 2002681.

[3] a) Q. Zhang, B. Li, S. Huang, H. Nomura, H. Tanaka, C. Adachi, *Nat. Photonics 2014*, *8*, 326; b) D. Zhang, M. Cai, Z. Bin, Y. Zhang, D. Zhang, L. Duan, *Chem. Sci*. **2016**, *7*, 3355; c) D. H. Ahn, H. Lee, S. W. Kim, D. Karthik, J. Lee, H. Jeong, J. Y. Lee, J. H. Kwon, *ACS Appl. Mater. Interfaces* **2019**, *11*, 14909.

[4] a) X. Cai, S.-J. Su, *Adv. Funct. Mater*. **2018**, *28*, 1802558; b) R. Braveenth, H. Lee, J. D. Park, K. J. Yang, S. J. Hwang, K. R. Naveen, R. Lampande, J. H. Kwon, *Adv. Funct. Mater.* **2021**, *31*, 2105805; c) P. Jiang, J. Miao, X. Cao, H. Xia, K. Pan, T. Hua, X. Lv, Z. Huang, Y. Zou, C. Yang, *Adv. Mater*. **2022**, *34*, 2106954; d) Z. Cai, X. Wu, H. Liu, J. Guo, D. Yang, D. Ma, Z. Zhao,B. Z. Tang, *Angew. Chem. Int. Ed*. **2021**,*60*, 23635; e) C. Han, R. Du, H. Xu, S. Han, P. Ma, J. Bian, C. Duan, Y. Wei, M. Sun, X. Liu, W. Huang, *Nat. Commun*. **2021**, *12*, 3640.

[5] A) L. Zhan, A. Ying, Y. Qi, K. Wu, Y. Tang, Y. Tan, Y. Zou, G. Xie, S. Gong, C. Yang, *Adv. Funct. Mater*. **2021**, *31*, 2106345; b) Y. Ran, G. Yang, Y. Liu, W. Han, G. Gao, R. Su, Z. Bin, J. You, *Mater. Horiz.* **2021**, *8*, 2025; c) X. Song, D. Zhang, Y. Lu, C. Yin, L. Duan, *Adv. Mater*. **2019**, *31*, 1901923; d) R. Braveenth, H. Lee, J. D. Park, K. J. Yang, S. J. Hwang, K. R. Naveen, R. Lampande, J. H. Kwon, *Adv. Funct. Mater*. **2021**, *31*, 2105805; e) C.-Y. Chan, M. Tanaka, Y.-T. Lee, Y.-W. Wong, H. Nakanotani, T. Hatakeyama, C. Adachi, *Nat. Photonics* **2021**, *15*, 203.

[6] D. Zhang, X. Song, A. J. Gillett, B. H. Drummond, S. T. E. Jones, G. Li, H. He, M. Cai, D. Credgington, L. Duan, *Adv. Mater*. **2020**, *32*, 1908355.

[7] a) H. Nakanotani, T. Higuchi, T. Furukawa, K. Masui, K. Morimoto, M. Numata, H. Tanaka, Y. Sagara, T. Yasuda, C. Adachi, *Nat. Commun*. **2014**, **5**, 4016; b) C. Yin, D. Zhang, Y. Zhang, Y. Lu, R. Wang, G. Li, L. Duan, *CCS Chem*. **2020**, *2*, 1268.

[8] a) N. C. Erickson, R. J. Holmes, *Adv. Funct. Mater*. **2013**, *23*, 5190; b) C. Zhang, Y. Lu, Z. Liu, Y. Zhang, X. Wang, D. Zhang, L. Duan, *Adv. Mater*. **2020**, *32*, 2004040.

[9] a) S. Kim, H. J. Bae, S. Park, W. Kim, J. Kim, J. S. Kim, Y. Jung, S. Sul, S.-G. Ihn, C. Noh, S. Kim, Y. You, *Nat. Commun*. **2018**, *9*, 1211; b) H. Wang, L. Meng, X. Shen, X. Wei, X. Zheng, X. Lv, Y. Yi, Y. Wang, P. Wang, *Adv. Mater*. **2015**, *27*, 4041; c) W. J. Chung, J. Y. Lee, *J. Mater. Chem. C* **2021**, *9*, 7458.

[10] J. Zeng, J. Guo, H. Liu, Z. Zhao, B. Z. Tang, *Adv. Funct. Mater*. **2020**, *30*, 2000019.

[11] a) Y. Fu, H. Liu, D. Yang, D. Ma, Z. Zhao, B. Z. Tang, *Sci. Adv*. **2021**, *7*, eabj2504; b) Y. Fu, H. Liu, D. Yang, D. Ma, Z. Zhao, B. Z. Tang, *Adv. Optical Mater*. **2022**, *10*, 2102339; c) R. Jiang, X. Wu, H. Liu, J. Guo, D. Zou, Z. Zhao, B. Z. Tang, *Adv. Sci*. **2022**, *9*, 2104435; d) R. Huang, H. Chen, H. Liu, Z. Zhuang, J. Wang, M. Yu, D. Yang, D. Ma, Z. Zhao, B. Zhong Tang, *Chem. Eng. J*. **2022**, *435*, 134934.

[12] a) J. Chen, J. Zeng, X. Zhu, J. Guo, Z. Zhao, B. Z. Tang, *CCS Chem*. **2021**, **3**, 230; b) Y. Luo, S. Zhang, H. Wang, Q. Luo, Z. Xie, B. Xu, W. Tian, *CCS Chem*. **2022**, *4*, 456; c) G. Yang, Y. Ran, Y. Wu, M. Chen, Z. Bin, J. You, *Aggregate* **2021**, e127.

[13] a) V. Jankus, P. Data, D. Graves, C. McGuinness, J. Santos, M. R. Bryce, F. B. Dias, A. P. Monkman, *Adv. Funct. Mater*. **2014**, *24*, 6178.; b) P. L. Dos Santos, J. S. Ward, M. R. Bryce, A. P. Monkman, *J. Phys. Chem. Lett*. **2016**, *7*, 3341; c) L. Zhan, Z. Chen, S. Gong, Y. Xiang, F. Ni, X. Zeng, G. Xie, C. Yang, *Angew. Chem., Int. Ed*. **2019**, *58*, 17651; d) J. Han, Y. Chen, N. Li, Z. Huang, C. Yang, *Aggregate* **2022**, e182.

[14] Z. S. An, J. S. Yu, S. C. Jones, S. Barlow, S. Yoo, B. Domercq, P. Prins, L. D. A. Siebbeles, B. Kippelen, S. R. Marder, *Adv. Mater*. **2015**, *17*, 2580.

[15] G. Lin, H. Peng, L. Chen, H. Nie, W. Luo, Y. Li, S. Chen, R. Hu, A. Qin, Z. Zhao, B. Z. Tang, *ACS Appl. Mater. Interfaces* **2016**, *8*, 16799.

[16] S.-J. Su, T. Chiba, T. Takeda, J. Kido, *Adv. Mater*. **2008**, *20*, 2125.

[17] P. M. Borsenberger, L. Pautmeier, R. Richert, H. Bässler, *J. Chem. Phys*. **1991**, *94*, 8276.

[18] W. S. Jeon, T. J. Park, S. Y. Kim, R. Pode, J. Jang, J. H. Kwon, *Org. Electron*. **2009**, *10*, 240.

[19] J. Kalinowski, W. Stampor, M. Cocchi, D. Virgili, V. Fattori, P. Di Marco, *Chem. Phys*. **2004**, *297*, 39.

[20] Baldo, M. A.; Adachi, C.; Forrest, S. R, *Phys. Rev. B*. **2000**, *62*, 10967.

[21] Reineke, S.; Walzer, K.; Leo, K, *Phys. Rev. B.* **2007**, *75*, 125328.

An efficient aggregation-enhanced delayed fluorescence luminogen (SBF-BP-SFAC) with balanced bipolar carrier transport and horizontal dipole orientation is developed, which provides outstanding external quantum efficiencies of up to 30.6% as emitter and 30.3% as sensitizer for orange fluorescence, phosphorescence and delayed fluorescence emitters with small efficiency roll-offs.